Analysis of Electrical Transport Properties of Amorphous Oxide Semiconductors by an Extended Percolation-Based Random Band-Edge Model

A. Welk,[*,‡] A. Reinhardt,[†,‡] O. Herrfurth,[§] D. Splith, H. von Wenckstern, and M. Grundmann

Universität Leipzig, Felix-Bloch-Institut für Festkörperphysik, Linnéstraße 5, Leipzig 04103, Germany

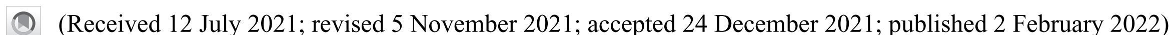

(Received 12 July 2021; revised 5 November 2021; accepted 24 December 2021; published 2 February 2022)

We investigate the electrical transport in amorphous oxide semiconductors by applying the percolation-based random band-edge model proposed by Nenashev *et al.* [Phys. Rev. B 100, 125202 (2019)] to multicationic, multianionic, and multinary materials. We modify the model by introducing the Hall-scattering factor. This allows us to evaluate, besides the conductivity, the temperature-dependent free charge-carrier concentration and Hall mobility, additionally enabling the inclusion of localized tail states in the model. The extended model allows analysis of pulsed-laser deposited amorphous zinc tin oxide, magnetron-sputtered amorphous zinc oxynitride, and zinc magnesium oxynitride thin films with carrier concentrations ranging from 10^{16} to 10^{19} cm^{-3} at room temperature. Excellent agreement of the extended model data with the measured electrical properties is found for the investigated temperature regime of 50 to 300 K. In addition, we extract critical parameters of the random band-edge model and discuss them with regard to varying deposition parameters and different anion and cation concentrations. In particular, we find the standard deviation of the mobility edge distribution to be ranging between 20 and 60 meV for the investigated materials.

DOI: 10.1103/PhysRevApplied.17.024007

I. INTRODUCTION

Research on amorphous oxide semiconductors (AOSs) has developed rapidly over the last two decades driven by the search for thin-film-transistor (TFT) channel materials suitable for the backplanes of transparent and flexible high-definition displays. AOSs show remarkable transport properties despite their disordered structure. In contrast to polycrystalline materials, the charge-carrier transport in AOSs is not limited by grain-boundary scattering and occurs via delocalized *s*-orbital states above the mobility edge [1]. In 2005, the amorphous multication compound zinc tin oxide (*a*-ZTO) and in 2009 the amorphous multianion compound zinc oxynitride (*a*-ZnON) with room-temperature electron mobility values up to 15 cm^2 V^{-1} s^{-1} and up to 100 cm^2 V^{-1} s^{-1}, respectively, have been proven to be indium-free alternatives to amorphous indium gallium zinc oxide (*a*-IGZO) for pixel drivers in active matrix displays [2,3]. Since then numerous studies on TFTs with isolated gates comprising these channel materials have been published. Besides, reports also exist on other devices, for instance, *a*-ZTO-based *p*-*n* diodes [4], Schottky diodes [5], metal-semiconductor field-effect transistors (MESFETs) [6,7] and more complex circuit elements as inverters [8,9] and ring oscillators [10]. And quite recently, we demonstrated *a*-ZnON-based MESFETs [11] and junction-gate field-effect transistors (JFETs) [12]. Despite considerable device research progress, a comprehensive description of charge-carrier transport in AOS materials is still under debate. Hopping and trap-limited transport in the sense of the conventional multiple trap and thermal release model have been thoroughly discussed for *a*-IGZO [13,14], *a*-ZTO [15,16], and *a*-ZnON [17], but these theories are hardly compatible with a properly measured Hall effect, without Hall sign anomaly, for free charge carriers with comparably large mobility values above 10 cm^2 V^{-1} s^{-1} in the investigated temperature regimes [18,19]. Several approaches have also been followed to explain the observed temperature dependence of the electrical conductivity $\sigma(T)$ and the thermally activated mobility for AOSs with the percolation theory applied to bandlike transport in extended states of a disordered system. The most established studies analyzing the charge transport in the framework of percolation theory in AOSs as *a*-IGZO presume a spatially varying potential landscape with random barrier heights above a distinct mobility edge [20–24]. However, this is in contrast to the assumption of the percolation approach by Adler *et al.* [25], which is

[*]antonia.welk@physik.uni-leipzig.de

[†]anna.reinhardt@physik.uni-leipzig.de

[‡]The authors contributed equally to this study.

[§]Present address: Active Fiber Systems GmbH, Ernst-Ruska-Ring 17, 07745 Jena, Germany.

 © 2022 American Physical Society

often quoted in this context. There, the absence of a sharp mobility edge in disordered semiconductors is emphasized. A brief description of the possible transport mechanisms in AOSs and their limitations are summarized in Ref. [26]. Further, the detailed theoretical description of the so-called random barrier model and its applicability to AOSs can be found in Ref. [27]. In their recent publication Nenashev *et al.* [26] proposed a percolation description for the random band-edge model suggested by Fishchuk *et al.* [19], which takes spatial variations of the mobility edge position due to structural disorder into account. The main difference between the analytical models of Adler *et al.*, Fishchuk *et al.*, and Nenashev *et al.* lies in the applied averaging procedures, which are also discussed in detail in Ref. [26]. In this paper, we examine the applicability of the random band-edge model formalism according to Nenashev *et al.* [26] to various AOS thin films aside from *a*-IGZO. For this purpose, we evaluate the electronic transport properties of the multication compound *a*-ZTO, the multianion compound *a*-ZnON and the combined multication and multianion compound zinc magnesium oxynitride (termed chemically nonexactly Zn-Mg-ON). In addition to the work of Nenashev *et al.*, we extend the model by considering the Hall-scattering factor in order to use besides temperature-dependent conductivity also Hall-effect data, free charge-carrier concentration and mobility, and thus reducing the number of degrees of freedom and enhancing the quality and reliability of the fit results. We show that it is possible to obtain consistent reliable physical quantities from the extended random band-edge model as: position of the Fermi level, intrinsic drift charge-carrier mobility, and most useful a band-disorder parameter describing the structural disorder in AOS materials. Since we increase the number of boundary conditions in the extended model compared to Nenashev *et al.*, we are able to include localized tail states and determine the density of localized states at the band edge as an additional parameter.

II. THEORETICAL MODEL DESCRIPTION

In the following, we briefly reproduce the theoretical description of the random band-edge (RBE) model by Nenashev *et al.* [26] and describe our own modifications. Under the assumption of random long-range potential fluctuations, described by a Gaussian distribution $G(E_m)$ of the mobility edge E_m with standard deviation δ, the electrical conductivity σ within the percolation approach is expressed as [26]

$$\sigma(T) = e\mu_0 n_{\text{mob}} = e\mu_0 \frac{1}{1-\vartheta_c}\int_{-0.95\delta}^{+\infty} G(E_m)dE_m \times \int_{E_m}^{+\infty} g(E-E_m)f(E)\,dE, \quad (1)$$

where $g(E-E_m)$, $f(E)$, μ_0, and ϑ_c denote the density of states (DOS) function, the Fermi function, the intrinsic drift charge-carrier mobility, and the percolation threshold [28], respectively. It should be noted that the temperature T enters only via the Fermi function. The DOS function $g(E-E_m)$ of AOSs is assumed to be close to that of crystalline semiconductors above E_m and having an exponential tail of localized states of the form $N_m \exp(E/E_0)$ below E_m.

The effective drift mobility μ is described by [26]

$$\mu = \mu_0 \frac{n_{\text{mob}}}{n_{\text{free}}}, \quad (2)$$

with n_{mob} being the concentration of mobile electrons dominating the percolation conductivity and n_{free} being the averaged total concentration of free electrons above the mobility edge E_m. The parameter μ_0 denotes the theoretical intrinsic drift charge-carrier mobility in the conduction band without potential fluctuations and is determined by the effective mass m^* and the average scattering time $\langle\tau\rangle$ in the classical Drude model for the electrical conductivity: $\mu_0 = e\langle\tau\rangle/m^*$. It has to be noted that, for the sake of simplicity, temperature-dependent scattering mechanisms are neglected and the parameter μ_0 is assumed to be independent of temperature in the RBE model. The theoretical derivation of these formulas according to Ref. [26] are described in more detail within the Supplemental Material [29]. Using the above formulas, the measured Hall-effect quantities can be formulated as follows:

$$\mu_{\text{Hall}}(T) = r_H \frac{\mu_0 n_{\text{mob}}}{n_{\text{free}}}, \quad (3)$$

$$n_{\text{Hall}}(T) = \frac{n_{\text{free}}}{r_H}. \quad (4)$$

This holds for the assumptions that the effective Hall conductivity ($e\mu_{\text{Hall}}n_{\text{Hall}}$) is similar to the percolation conductivity ($e\mu n_{\text{free}}$) and that the Hall voltage signal is similar to that in homogeneous semiconductors. Note that this is only valid for the case of weak disorder ($\delta \to 0$) [19,30]. The so-called Hall-scattering factor, which relates Hall mobility and carrier concentration to the drift mobility and free electron concentration, is defined by $r_H = \langle\tau^2\rangle/\langle\tau\rangle^2$ [31]. Typical values for crystalline semiconductors range between $r_H = 1$ for energy-independent scattering mechanisms (for degenerate carrier concentrations) and $r_H = 1.93$ if ionized impurity scattering is dominant (for nondegenerate carrier concentrations) [32]. Therefore, we fix r_H in the range of 1–2, if possible, and consequently neglect its temperature dependence. If the Fermi level E_F lies above E_m or not more than $4k_BT$ below the mobility edge (degeneracy criteria), r_H is assumed to be unity. In the present model, the position of E_F is zero for the mean mobility edge $\langle E_m\rangle$ and is defined by the total charge-carrier concentration n_{total} of the semiconductor, which is

the sum of electrons in localized states below E_m as well as in extended states above E_m averaged over the E_m distribution [19] (see Supplemental Material [29]). The value of n_{total} is usually not known in AOSs, since unintentional n-type doping is mainly caused by undercoordinated cations and therefore the value of E_F depends on film growth conditions and postgrowth processes like annealing [33] or plasma treatment [34], which in turn also affect the cationic and anionic disorder, respectively. Besides, the undercoordination in AOSs can also be influenced under bias illumination stress [35]. Since the value of n_{total} and its temperature dependence, respectively, is not available from the conducted experiments, we *a priori* assume the Fermi level E_F to be temperature independent for the whole investigated temperature regime from 50 to 300 K. Implications of this simplification are discussed later on.

In summary, we use Eqs. (1)–(4), with the interdependence $\sigma = e\mu_{\text{Hall}}n_{\text{Hall}}$, yielding four parameters μ_0, δ, E_F, and N_m, in order to fit the experimentally determined electrical properties σ, μ_{Hall}, n_{Hall} via a nonlinear least-squares algorithm. In contrast to the density of localized states parameter N_m, the parameter E_0 describing the width of the exponential band tails is assumed to be constant with a value of about $E_0 = 30$ meV, which is a good estimate at least for *a*-ZTO [36] and *a*-ZnON [17]. We note that it would be sufficient to fit only the Hall mobility and carrier concentration in order to determine the model parameters. But the signal-to-noise ratio of the Hall-effect quantities can become small at low temperatures, especially for more resistive samples, providing a much smaller temperature range than the measured sheet resistance. Therefore, in order to ensure a larger fit range, the electrical conductivity σ is also included in the fit function. Details on the fit routine can be found within the Supplemental Material [29].

On a final note, as the parameter δ specifies the width of the Gaussian band-edge distribution, it is a direct measure of the degree of disorder introduced at the conduction-band edge and is therefore called the band-disorder parameter in the following.

III. EXPERIMENTAL DETAILS

A. Thin-film deposition

All thin films are deposited on 10×10 mm^2 Corning borosilicate glass substrates. The *a*-ZTO thin films are fabricated by means of pulsed-laser deposition (PLD) at room temperature. One sample set is ablated from a ceramic target composed of 33 mol% ZnO and 67 mol% SnO_2 corresponding to a zinc-to-tin cation ratio of 1:2 at different oxygen partial pressures $p(O_2)$, varied between 3.0×10^{-2} mbar to 3.8×10^{-2} mbar. A second sample set of *a*-ZTO thin films with varying cation compositions is ablated from targets composed of ZnO and SnO_2 with ratios of 1:2, 1:1, and 2:1 at a constant $p(O_2) = 3.0 \times 10^{-2}$ mbar.

For *a*-ZnON, we reuse the temperature-dependent Hall-effect data from Reinhardt *et al.* [37] These *a*-ZnON thin films are rf sputtered at different substrates temperatures from a metallic Zn target in a reactive $Ar/N_2/O_2$ gas atmosphere using a long-throw magnetron sputtering system from Mantis Deposition. More details can be found in Ref. [37].

The Zn-Mg-ON thin films, as a multinary compound, are fabricated with the same magnetron sputtering setup as *a*-ZnON but with an additional magnesium target for cosputtering. Magnesium cation compositions between 2 and 5 at.% are achieved leading to a decrease in charge-carrier concentration compared to *a*-ZnON as described in detail in Ref. [38].

B. Electrical characterization

The four-point probe van der Pauw method is used for temperature-dependent resistivity and Hall-effect measurements on *a*-ZTO, *a*-ZnON, and Zn-Mg-ON thin films with dc-sputtered Ohmic Au contacts placed on the corners of the sample. For *a*-ZTO and Zn-Mg-ON, those measurements are performed with a Quantum Design Physical Property Measurement System using a magnetic field of 1 T. The electrical characterization of *a*-ZnON thin films is conducted with a home-built Hall-effect measurement setup with a magnetic field of 0.43 T.

IV. RESULTS

A. Model verification

In order to validate the extended RBE model, we firstly apply it to the same *a*-IGZO reference data [22,23] as Nenashev *et al.* [26]. Following Ref. [26], we use an effective mass of 0.34 m_e, which is estimated from the free-carrier absorption of degenerate *a*-IGZO [22], and neglect localized states below the mobility edge by setting $N_m = 0$. In contrast to Nenashev *et al.*, we do not assume a fixed parameter set μ_0 and δ for the sample ensemble. Instead, we fit the curves with individual optimized fit parameters E_F, μ_0, and δ since, as already mentioned above, a change in the n-type doping cannot be considered independently from the introduced cationic disorder in AOSs. For the interested reader, results from a multisample fit with fixed δ are shown within the Supplemental Material [29]. To reduce the number of fit parameters to a minimum, we fix the Hall-scattering factor at $r_H = 1$. The model parameters E_F and δ are only slightly correlated with r_H, in contrast to the parameters μ_0 and N_m (if considered) that show a non-negligible dependence on the Hall-scattering factor. Thus the obtained value of μ_0 for $r_H = 1$ displays the upper limit for the intrinsic band mobility. More details on the

influence of the Hall-scattering factor can be found within the Supplemental Material [29].

The obtained fit curves are presented in Figs. 1(a)–1(c) as solid lines. It can be seen that while the model curves of the IGZO thin films, labeled with $a1$ and $a2$, are in agreement with the experimental data, the thin films with low free electron concentration ($a3$ and $a4$) exhibit deviations from the model, indicating its limitations. In particular, the assumption of a constant Fermi level over the whole temperature range is not tenable for the samples $a3$ and $a4$. However, for the determination of the parameters μ_0 and δ the neglection of the E_F temperature dependence plays only a minor role (see Supplemental Material [29]). It should also be emphasized that when modeling conductivity data only, it is possible to obtain mathematically better fit results with the smallest deviations for all a-IGZO samples as presented within the Supplemental Material [29]. However, our experience with various AOS materials has shown that in most cases no physically meaningful parameter values for μ_0 and δ can be achieved by modeling only the conductivity, whereas the extended model leads to physically plausible results for all investigated AOSs, as shown later on.

The resulting fit parameters for a-IGZO are shown in Fig. 1(d) and are summarized in Table I. As the model parameters E_F and δ are cross-correlated, it is not possible to identify unique parameter values within reasonable uncertainty limits for the temperature-independent transport data of the highly degenerate a-IGZO thin film ($a1$). The presented fit curve is thus obtained by fixing δ at 25 meV as obtained from the multisample fit. Due to the same argumentation, the calculated best-fit parameters for the sample $a2$ (without fixing δ) are clearly outlier overestimating μ_0 and δ. Even if considering the temperature dependence of E_F or limiting the fit range to the low-temperature region, where a constant E_F is a good approximation, it is not possible to fit the whole data set satisfactorily with reasonable parameter values. Overall, the inclusion of measurement errors would help to increase the confidence level of the fit parameters, but unfortunately such data are not available here. We note that such ambiguities do not occur when modeling our experimental data. However, as the obtained E_F values are close to the mean mobility edge (within $4k_BT$), the assumption of $r_H = 1$ is reasonable and the obtained μ_0 values should be realistic estimates for the intrinsic band mobility of a-IGZO, in the

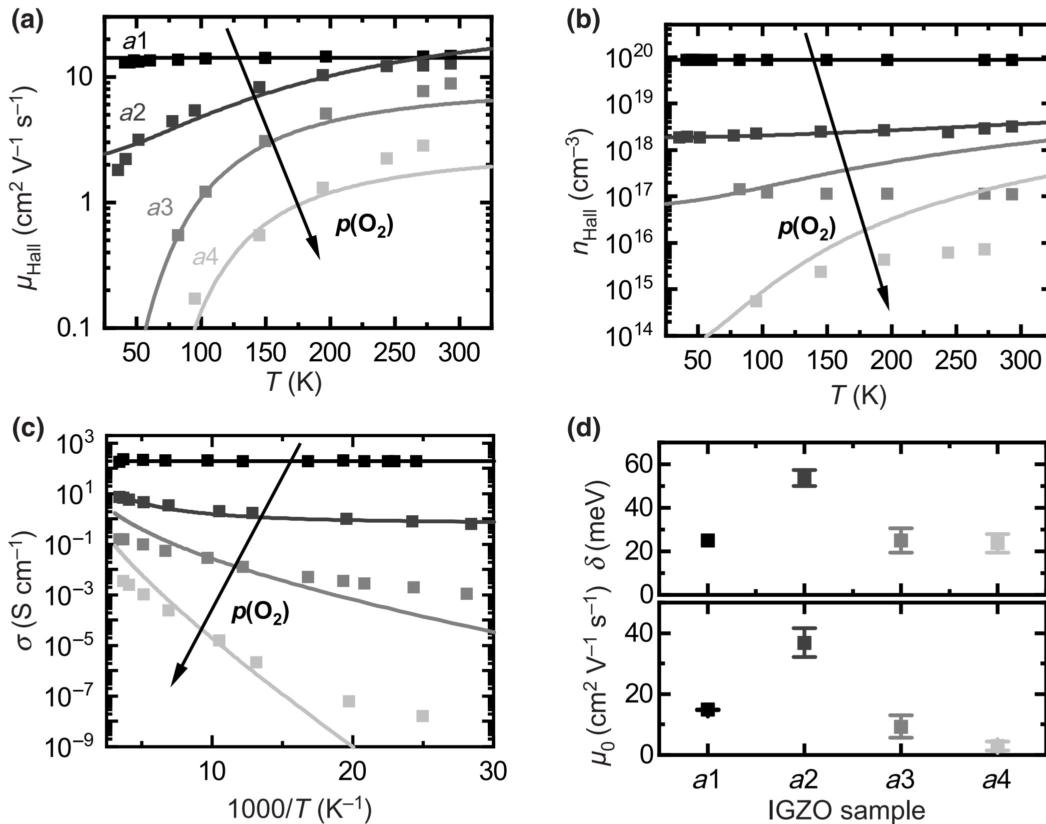

FIG. 1. Results of modeling the temperature-dependent Hall mobility μ_{Hall} (a), Hall electron concentration n_{Hall} (b), and corresponding electrical conductivity σ (c) according to the extended RBE model for a-IGZO thin films deposited by means of PLD with oxygen partial-pressure variation $p(O_2)$ as indicated by the arrow: data (symbols) adopted from Takagi *et al.* [22] and fit curves (solid lines). (d) Resulting best fit parameters δ and μ_0. The error bars indicate the fit errors.

TABLE I. Fit parameters for the individually modeled Hall mobility, free-carrier concentration, and conductivity of *a*-IGZO thin films shown in Fig. 1.

a-IGZO	E_F (meV)	δ (meV)	μ_0 (cm^2 V^{-1} s^{-1})	N_m (cm^{-3} eV^{-1})	r_H	m^* (m_e)
*a*1	210	25	15	···	1	0.34
*a*2	−32	54	37	···	1	0.34
*a*3	−40	25	9.3	···	1	0.34
*a*4	−92	24	2.9	···	1	0.34

case of correctly chosen E_F and δ values. Since no values for the Fermi level are published in Ref. [26] and the results for μ_0 and δ are only given for the whole sample ensemble, a direct parameter comparison for each model curve is not possible, only mean values can be compared. The mean values of our fit parameters, $\overline{\delta} = 32$ meV and $\overline{\mu}_0 = 16$ cm^2 V^{-1} s^{-1}, compared to the values $\delta = 36$ meV and $\mu_0 = 47$ cm^2 V^{-1} s^{-1} published in Nenashev *et al.* [26], show an excellent agreement for the band-disorder parameter δ but a strong deviation for the intrinsic band mobility μ_0. This deviation is related to the differences in the modeling approaches, in particular, to the Hall-scattering factor. Due to the mentioned parameter correlations in the RBE model, fitting only the conductivity data, and with that ignoring the Hall-scattering factor, can lead to significant over- or underestimation of the parameter μ_0 (see Supplemental Material [29] for more details). The additional boundary condition of $r_H = 1$ prevents such incorrect estimates. Therefore, the herein obtained $\overline{\mu}_0$ compares well with the result of Fishchuk *et al.* [19], $\delta = 40$ meV and $\mu_0 = 14$ cm^2 V^{-1} s^{-1}, who also considered the Hall-scattering factor for modeling the same *a*-IGZO data based on an effective medium approximation of the RBE model. The differences in δ can be assigned to different assumptions on the value of the total carrier concentration in the system, which determine E_F.

In summary, it is shown that the presented approach is capable of obtaining reasonable values for the disorder parameters μ_0 and δ within the discussed uncertainties. Moreover, we can now apply our extended percolation-based RBE model to temperature-dependent electrical transport data of various AOS materials and correlate different growth conditions with the degree of disorder introduced at the conduction-band edge.

B. Modeling of *a*-ZTO thin-film conductivity

The effect of cationic disorder in *a*-ZTO is investigated by modeling temperature-dependent Hall-effect data, shown in Fig. 2, of *a*-ZTO thin films deposited under nominal identical conditions from targets with varying zinc-to-tin cation ratio Zn/Sn of 1:2, 1:1, and 2:1. Regarding the cation ratio in the as-deposited thin films, we observe a favorable tin-atom transfer from the PLD target into the growing films compared to zinc atoms. Due to their higher atomic mass, scattered tin atoms are deflected less on their way towards the substrate compared to the lighter zinc atoms. Therefore, the corresponding zinc-to-tin cation ratios in the deposited thin films are with 1:2.3, 1:1.1, and 2:1.3, respectively, slightly lower than in the PLD target, which is confirmed by energy dispersive x-ray spectroscopy (EDX) measurements and is in agreement with former studies [39]. In the following, given Zn/Sn ratios refer to the target composition.

Theoretical calculations predict an effective electron mass m^* of 0.18 $m_e - 0.19$ m_e for $c - \mathrm{ZnSnO_3}$ [40] and 0.23 $m_e - 0.26$ m_e for $c - \mathrm{Zn_2SnO_4}$ [41], which are slightly increased in the corresponding amorphous compounds [42]. Thus, for modeling we assume a value of 0.2 m_e for Zn/Sn $= 1:1$ and 0.3 m_e for the other cation ratios. We note that the choice of m^* has only a minor influence on the fit parameters in the present model, except for the choice of r_H and with that μ_0, as shown below.

The corresponding fit parameters are plotted in Fig. 2(d) as a function of the cation ratio and are summarized in Table II. For Zn/Sn $= 1:1$ and 2:1 we find similar low δ values of about 22 meV. In accordance with several theoretical and experimental studies, indicating a (nonuniform) structural disorder increase with increasing Sn content in *a*-ZTO [42,43], we obtain the highest band-disorder parameter δ between 40–60 meV for *a*-ZTO thin films with $\mathrm{Sn/(Sn + Zn)} \approx 70\%$, the highest amount of Sn atoms. The density of localized states at the band edge N_m is found to range between (0.11–1.50) $\times 10^{20}$ cm^{-3} eV^{-1}, which is consistent with tail-state densities extracted from temperature-dependent current-voltage measurements on ZTO thin-film diodes and transistors, respectively [16,36]. Besides, similar fit parameters are obtained if localized tail states are neglected by setting $N_m = 0$ (see Table II). The largest N_m values are observed for Zn/Sn ratios of 1:2 and 2:1. This can be explained by undercoordinated metal atoms mainly causing localized states below the conduction-band minimum, especially in oxygen-poor compositions [42,44].

In order to corroborate these result, we also evaluate Hall-effect data of *a*-ZTO thin films deposited from a PLD target with Zn/Sn $= 1:2$ under different oxygen partial pressures $p(\mathrm{O_2})$ (see Fig. 3 and Table II). Indeed, we find that the density of localized states at the band edge decreases with increasing $p(\mathrm{O_2})$ as well

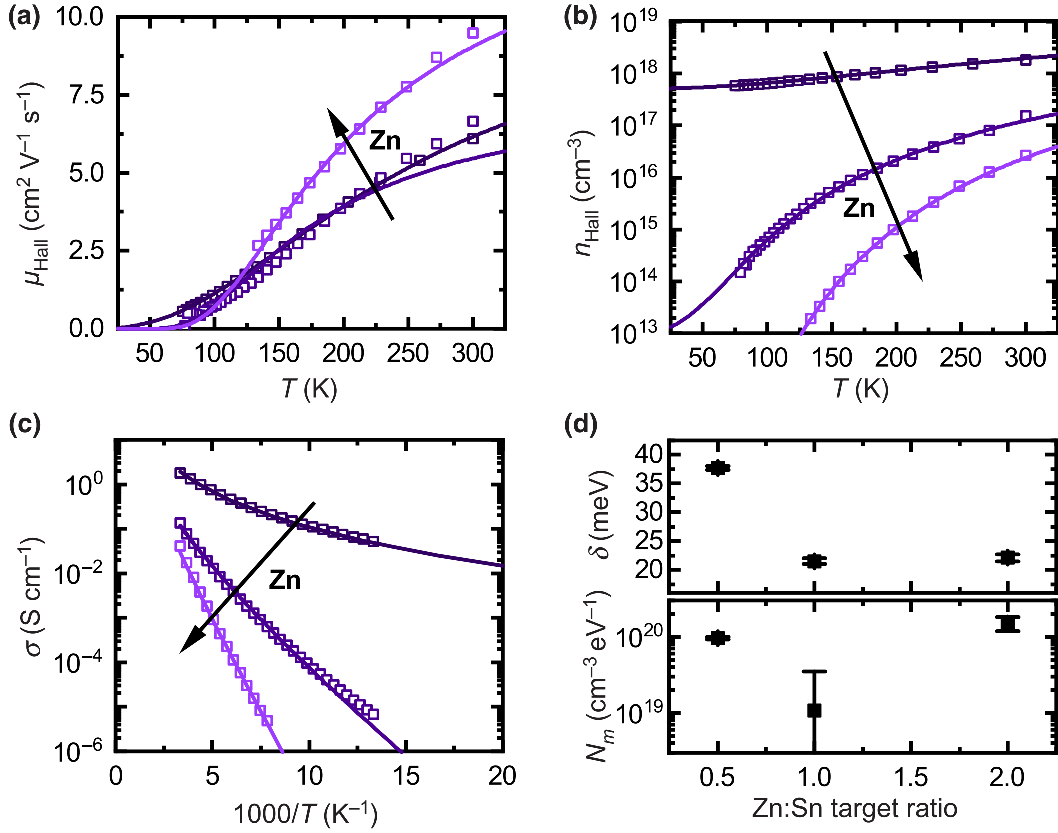

FIG. 2. Results of modeling the temperature-dependent Hall mobility μ_{Hall} (a), Hall electron concentration n_{Hall} (b), and corresponding electrical conductivity σ (c) according to the random band-edge model [Eq. (1)] for *a*-ZTO thin films deposited from PLD targets with various zinc-to-tin cation ratios of 1:2, 1:1, and 2:1: measured data (symbols) and fit results (solid lines). (d) Obtained band-disorder parameter δ and density of localized states at the band edge N_m in dependence on the target cation ratio. All fit parameters are summarized in Table II.

as the band-disorder parameter δ, which is attributed to the reduction of oxygen deficiency. A significant change of the cation ratio with $p(O_2)$ can be excluded in this narrow deposition pressure window, confirmed by EDX. Theoretical as well as experimental studies confirmed that reducing anion deficiency in *a*-ZTO, which coincides with a reduced amount of oxygen-vacancy related defects, results in a reduction of deep as well as conduction band-edge-near-subgap states originating from undercoordinated cations [44,45]. Therefore, an oxygen partial-pressure increase results in a reduced *a*-ZTO thin-film conductivity. The decrease of δ with increasing $p(O_2)$ can be understood as a reduction of spatially random atomic distance variations, which are presumably caused

TABLE II. Fit parameters for the modeled Hall mobility and free-carrier concentrations of *a*-ZTO thin films shown in Figs. 2 and 3 in dependence on the cation ratio and the deposition pressure $p(O_2)$, respectively. Values in parentheses denote the obtained fit parameter if localized tail states are neglected ($N_m = 0$).

a-ZTO	E_F (meV)	δ (meV)	μ_0 (cm^2 V^{-1} s^{-1})	N_m (cm^{-3} eV^{-1})	r_H	m^* (m_e)
Zn/Sn ratio						
1:2	−40 (−38)	38 (41)	12 (13)	1.0×10^{20}	1	0.3
1:1	−82 (−82)	22 (22)	8.4 (8.3)	1.1×10^{19}	1	0.2
2:1	−156 (−148)	22 (23)	14 (14)	1.5×10^{20}	1	0.3
$p(O_2)$ (10^{-2} mbar)						
3.0	−38	58	20	7.0×10^{20}	1	0.3
3.5	−39	33	9.4	4.6×10^{19}	1.6	0.3
3.8	−87	27	2.0	$<1 \times 10^{19}$	4	0.3
3.8	−90	27	4.3	$<1 \times 10^{19}$	2	0.2

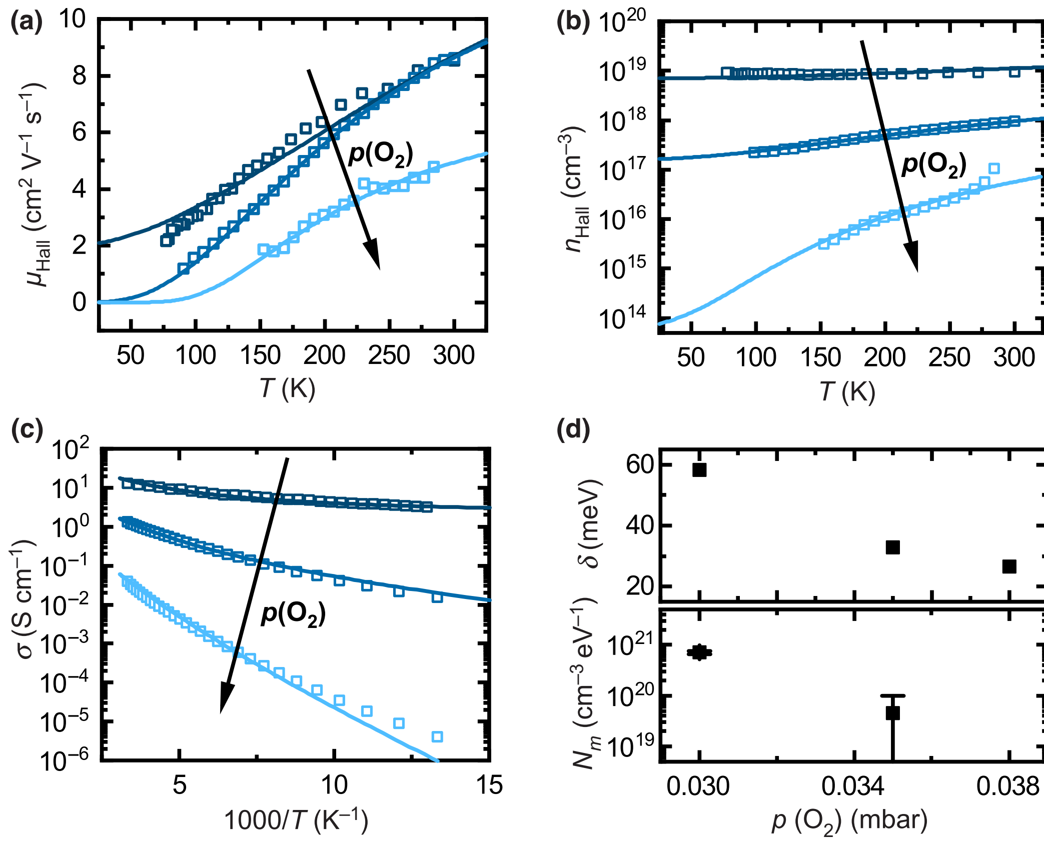

FIG. 3. Results of modeling the temperature-dependent Hall mobility μ_{Hall} (a), Hall electron concentration n_{Hall} (b) and corresponding electrical conductivity σ (c) according to the random band-edge model [Eq. (1)] for *a*-ZTO thin films deposited at different oxygen partial pressures $p(O_2)$ from a PLD target with 1:2 Zn/Sn ratio: measured data (symbols) and fit results (solid lines). (d) Obtained band-disorder parameter δ and density of localized states at the band edge N_m in dependence on the oxygen partial pressures $p(O_2)$. All fit parameters are summarized in Table II.

by the nonuniform distribution of tin atoms with different coordination number.

As the obtained parameter value for the intrinsic mobility μ_0 depends on the choice of r_H, it has the largest absolute uncertainties. Nevertheless, the calculated values for $r_H = 1$ are comparable and in a reasonable range of $\mu_0 = 8$–20 cm^2 V^{-1} s^{-1} for *a*-ZTO. Also, the observed trend is in agreement with other reports on the dependence of electron transport on the cation ratio in *a*-ZTO. In particular, Siah *et al.* showed that a mobility reduction is correlated with increasing structural disorder due to Sn increase in Zn-rich *a*-ZTO, whereas mobility increases again in Sn-rich *a*-ZTO thin films [43]. The former is attributed to a reduced hybridization strength between Zn4*s* and O2*p* orbitals and the latter to the larger ionic radii of the Sn5*s* orbitals predominating the electron conduction paths [42,43].

For the pressure series it is not possible to fit the whole Hall-effect data set with $r_H = 1$. In particular, fitting with $m^* = 0.3\ m_e$ delivers $r_H = 4$ for the most resistive *a*-ZTO thin film deposited at $p(O_2) = 3.8 \times 10^{-2}$ mbar. Interestingly, a more reasonable r_H value of 2, which is expected if ionized impurity scattering is dominant, can only be modeled with lower effective mass $m^* = 0.2\ m_e$. In both cases the obtained values for N_m are below 10^{19} cm^{-3} eV^{-1}, which is negligible. It can be seen that the intrinsic mobility μ_0 is underestimated by a factor of 2 at most if $r_H = 4$ is considered, whereas the other fit parameters do not significantly change. Nevertheless, irrespective of r_H, a decrease of μ_0 is observed with increasing oxygen partial pressure, which could be explained by a reduced Sn5*s* orbital overlap or other additional scattering sources limiting the electron mean free path in the extended states. Due to the deposition at room temperature it is quite likely that there are some inhomogeneities in the growing amorphous thin film. Possible local microstructural inhomogeneities or spatial variations in cation distributions are not detectable with EDX. Also, the formation of local nanocrystalline phases causing additional spatial potential fluctuations or scattering centers cannot be excluded for certain, but all investigated *a*-ZTO thin films are at least X-ray amorphous.

In summary, except for the discussed uncertainty for the most resistive ZTO sample, we can conclude that the

present extended random band-edge model is adequate for quantitative modeling of the temperature dependence of Hall mobility and carrier concentration in multicationic AOSs. The obtained model parameters and their correlations regarding deposition conditions for *a*-ZTO thin films are in agreement with the existing literature.

C. Modeling of *a*-ZnON thin-film conductivity

As the measured Hall-effect data for *a*-ZnON thin films show a percolation conduction behavior similar to multicationic AOSs, we also evaluate the application of the extended random band-edge model to this multianion AOS. It is obvious that long-range potential fluctuations in a single-cation AOS like *a*-ZnON can not be ascribed to an inhomogeneous distribution of multiple metal cations with different ionic radii. Nevertheless, spatial inhomogeneities are expected due to the following explanation: the amorphous nature of ZnON results from the competition of different crystal structures, namely hexagonal ZnO and cubic Zn_3N_2, during the sputtering process from a metallic Zn target with two reactive gases O_2 and N_2. Further, due to the much higher reactivity of oxygen compared to nitrogen a careful control of the oxygen partial pressure is necessary in order to ensure a sufficient nitrogen incorporation in the thin film and prevent target oxidation during reactive sputtering. Thus, spatial inhomogeneities like density and compositional fluctuations or even nanocrystalline regions in the as-deposited thin films can easily occur during oxynitride synthesis and it needs precise anion control to avoid them. Several experimental studies employing high-resolution transmission electron microscopy confirmed the inhomogeneous nature of ZnON thin films depending on anion ratios and deposition conditions, respectively [46–48]. Therefore, the application of a random band-edge model for this single-cation AOS is justified.

In Fig. 4 the fit results for as-deposited *a*-ZnON thin films with varying free carrier concentrations between 7×10^{17} cm^{-3} and 5×10^{18} cm^{-3}, depending on the deposition temperature T_S, are depicted. The extended random band-edge model fits the data well yielding reasonable model parameters as exemplarily presented in Fig. 4(d) and summarized in Table III. For modeling, we assume an effective electron mass of 0.2 m_e for *a*-ZnON [17,49]. In contrast to *a*-ZTO, a non-negligible density of localized

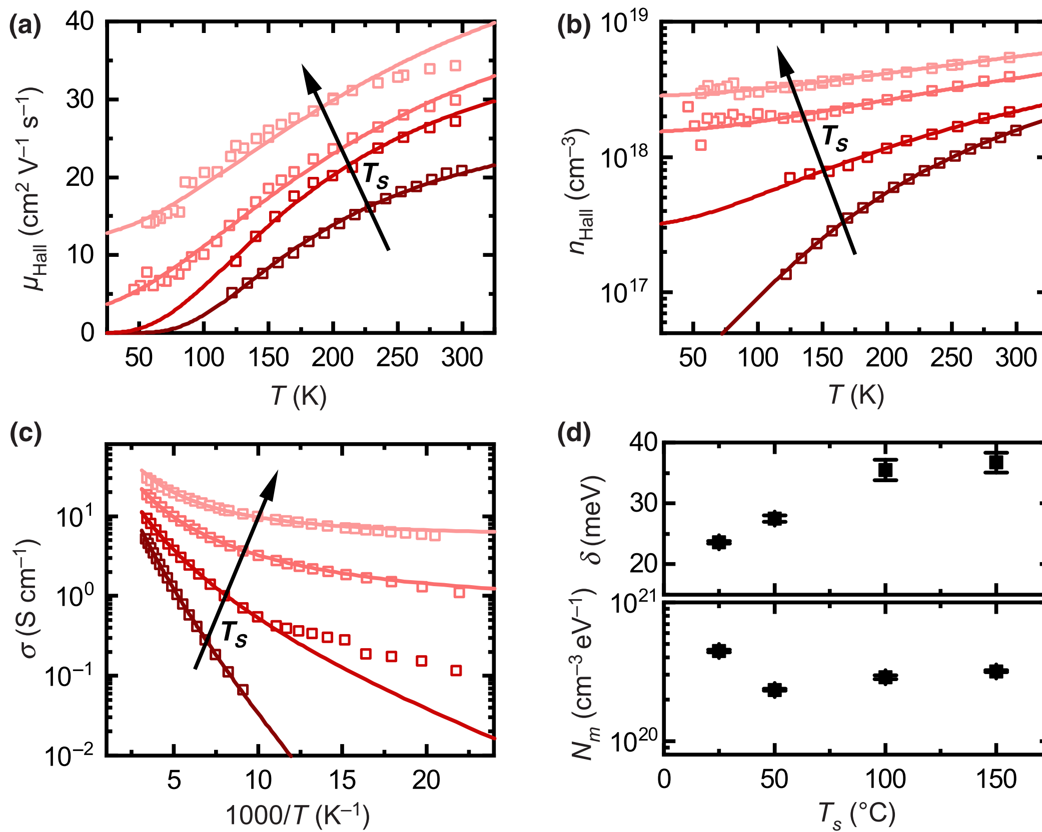

FIG. 4. Results of modeling the temperature-dependent Hall mobility μ_{Hall} (a), Hall electron concentration n_{Hall} (b), and corresponding electrical conductivity σ (c) according to the random band-edge model [Eq. (1)] for *a*-ZnON thin films deposited at different substrate temperatures T_S: measured data (symbols) and fit results (solid lines). (d) Obtained band-disorder parameter δ and density of localized states at the band edge N_m in dependence on the substrate temperature T_S. All fit parameters are summarized in Table III.

TABLE III. Fit parameters of the modeled Hall-effect data shown in Fig. 4 of *a*-ZnON thin films deposited at different substrate temperatures T_S.

a-ZnON	E_F (meV)	δ (meV)	μ_0 (cm^2 V^{-1} s^{-1})	N_m (cm^{-3} eV^{-1})	r_H	m^* (m_e)
T_S (°C)						
Room temperature	−61	24	32	4.5×10^{20}	1	0.2
50	−37	28	44	2.3×10^{20}	1	0.2
100	−27	36	53	2.9×10^{20}	1	0.2
150	−17	36	60	3.2×10^{20}	1	0.2

states at the band edge N_m in the order of 10^{20} cm^{-3} eV^{-1} at the conduction-band edge has to be considered in this case in order to adequately fit the Hall-effect data of *a*-ZnON thin films with a Hall-scattering factor of $r_H = 1$. This is in agreement with the observation of trap-limited conduction in *a*-ZnON channel TFTs, where the effective field-effect mobility is affected by charge-carrier trapping in localized conduction-band tail states [17,50]. Furthermore, our determined fit values correspond well with the extracted density of 2×10^{20} cm^{-3} eV^{-1} from TFT transport measurements reported by Lee *et al.* [17]. Such localized tail states below the conduction-band minimum in *a*-ZnON are attributed to nitrogen-related defects, like nonstoichiometric Zn_xN_y bonds or N-N dimers, and therefore their density strongly depends on the anion composition and chemical bonding states [46,48,51]. For N-rich ZnON films with N/(N+O) $\geq$ 60% Jang *et al.* showed that the exponential density of tail states, extracted from monochromatic photonic capacitance-voltage measurements on ZnON TFTs, decrease with increasing N content, whereas a Gaussian-distributed shallow donor level peaking at 0.15 eV below the conduction-band minimum, attributed to nitrogen vacancies, clearly arises for N/(N+O) $\geq$ 80% [48,52].

From modeling of the measured temperature dependence of *a*-ZnON conductivity and Hall-effect data, we find that the density of localized tail states at the conduction-band edge significantly decreases when going from room-temperature deposition to 50 °C substrate temperature, suggesting an improved nitrogen incorporation in the growing thin film according to the above explanations. N_m increases again with further substrate temperature increase, which in turn suggests the out diffusion of loosely bound nitrogen. Further, we observe a slight increase of the band-disorder parameter δ from 24 to 36 meV and almost a doubling of μ_0 from 32 to 60 cm^2 V^{-1} s^{-1} with increasing deposition temperature T_S for *a*-ZnON thin films. These findings indicate, on the one hand, an increase of global disorder introduced to the mobility edge and, on the other hand, a local disorder decrease resulting in an increased intrinsic mobility μ_0.

The above results may be interpreted to result from the reduction of loose metal-anion bonds by providing additional thermal energy, which likely reduce defect states and scattering centers, but also promotes the formation of nonuniformly distributed nanocrystalline phases in the mainly amorphous films [47,51]. However, this cannot be clarified for certain without additional experimental information on the microstructure and the chemical bonding states.

Nevertheless, the temperature dependence of the electrical conductivity, Hall mobility, and free-carrier concentration of rf-sputtered *a*-ZnON thin films can be satisfactorily modeled with the extended random band-edge model including tail states with a reasonable small band-disorder parameter δ of 24–36 meV as expected for a single-cation AOS. Furthermore, this analysis of transport measurements by applying the random band-edge model in combination with other characterization methods could provide a valuable tool to shed a light on the complex nature of electron transport in *a*-ZnON covering trap-limited and percolation conduction mechanisms.

D. Modeling of Zn-Mg-ON thin-film conductivity

Besides multianion and multication AOS materials we investigate the validity of the extended random band-edge model for the combined multianion and multication compound Zn-Mg-ON. The electrical, optical, and structural properties of this AOS material have been discussed thoroughly in Ref. [38]. The temperature-dependent Hall-effect data for samples with varying magnesium cation concentrations between 2 and 5 at.% are modeled including non-negligible localized tail states and with a Hall-scattering factor of $r_H = 1$ as for *a*-ZnON for a useful comparison. For further results with $r_H > 1$ see Supplemental Material [29]. The effective mass is slightly adjusted due to the additional magnesium cations contributing to conduction-band states. We choose $m^* = 0.3\ m_e$ as a rough estimate taking into consideration the effective mass of pure *a*-ZnON $m^* = 0.2\ m_e$ and the effective mass of Zn-Mg-O $m^* = (0.2 - 0.5)\ m_e$, which varies strongly depending on the magnesium content and from publication to publication [53,54]. The fit results are presented in Figs. 5(a)–5(c) and the corresponding fit parameters are depicted in Fig. 5(d) and in Table IV. We observe that the density of localized states at the band edge is insignificantly larger for the

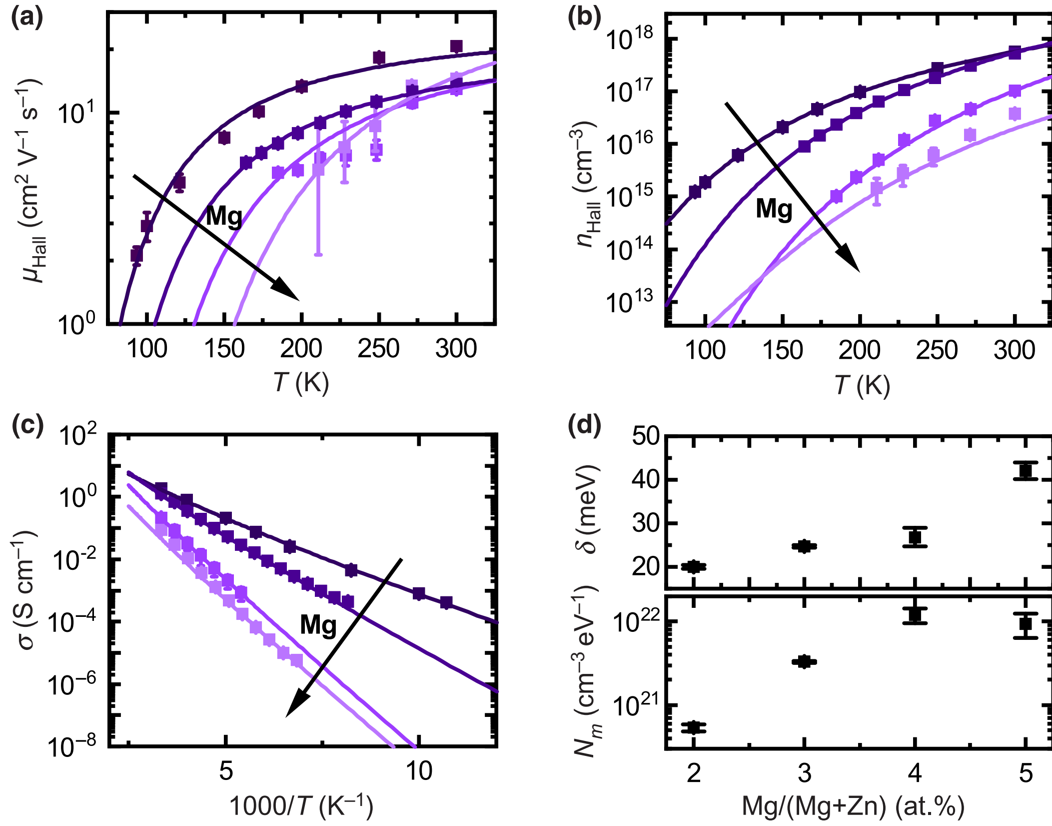

FIG. 5. Results of modeling the temperature-dependent Hall mobility μ_{Hall} (a), Hall electron concentration n_{Hall} (b), and corresponding electrical conductivity σ (c) according to the random band-edge model [Eq. (1)] for Zn-Mg-ON thin films fabricated with magnetron co-sputtering a magnesium cation concentration between 2 and 5 at.%: measured data (symbols) and fit results (solid lines). (d) Obtained band-disorder parameter δ and density of localized states at the band edge N_m. All fit parameters are summarized in Table IV.

Zn-Mg-ON thin films with 2 at.% magnesium content $N_m = 5.3 \times 10^{20}$ cm^{-3} eV^{-1} compared to the results of *a*-ZnON $N_m = 4.5 \times 10^{20}$ cm^{-3} eV^{-1} at room temperature. Further, the localized tail-state density significantly increases with increasing magnesium content from 2 at.% up to 4 at.%. This effect might be assigned to differences in anion composition. Due to the strong oxidation potential of the magnesium target, magnesium addition leads to a correlated increase in the oxygen and decrease in the nitrogen content as known from Ref. [38]. This change from the nitrogen-rich *a*-ZnON with N/(N+O) $\approx$ 60% to the oxygen-rich Zn-Mg-ON phase with N/(N+O) $\leq$ 50% leads to less nitrogen-zinc bonds and therefore to more nitrogen-related tail states.

Furthermore, the global disorder increases from $\delta = 20$ to 42 meV. This can be assigned to an inhomogeneous distribution of metal zinc and magnesium cations causing enhanced potential fluctuations of the mobility edge. Up to a magnesium content of 4 at.% the intrinsic mobility decreases from 27 cm^2 V^{-1} s^{-1} to 19 cm^2 V^{-1} s^{-1}. This might be explained by a local disorder increase due to additional magnesium cations in the Zn-Mg-ON amorphous matrix. For even higher magnesium concentrations of 5 at.% the intrinsic mobility increases significantly up

TABLE IV. Fit parameters for the modeled Hall mobility, free-carrier concentration, and conductivity of Zn-Mg-ON thin films shown in Fig. 5 in dependence on the magnesium content Mg/(Mg + Zn).

Zn-Mg-ON	E_F (meV)	δ (meV)	μ_0 (cm^{2}V^{-1}s^{-1})	N_m (cm^{-3}eV^{-1})	r_H	m^* (m_e)
Mg/(Mg + Zn) (at. %)						
2	−91	20	27	5.3×10^{20}	1	0.3
3	−143	25	23	3.3×10^{21}	1	0.3
4	−218	27	19	1.2×10^{22}	1	0.3
5	−263	42	52	9.4×10^{21}	1	0.3

to 52 $cm^2 V^{-1} s^{-1}$. Certainly, the Hall-scattering factor should not be close to unity for the obtained Fermi level. For $r_H = 2$ the determined intrinsic mobility value is 25 $cm^2 V^{-1} s^{-1}$. Since the Zn-Mg-ON thin films with 5 at% Mg are no longer X-ray amorphous and crystalline magnesium oxide and zinc oxide phases are present [38], the intrinsic band mobility might be comparable to the in-grain mobility of ZnO with local crystalline order, whereas on the global scale grain boundaries cause additional potential fluctuations and therewith lead to an increased long-range disorder.

V. DISCUSSION

There are some uncertainties of the model parameters that have to be taken into consideration when interpreting the presented results. As already mentioned, uncertainties in the assumptions made on the values of m^*, r_H, and N_m can give rise to relatively large uncertainties in the extracted fit parameters due to the inherent interdependence of the parameters of the model functions. In particular, an underestimation of the effective mass m^*, which determines the effective DOS at the mobility edge, can easily result in an overestimation of the localized tail-state density N_m at the mobility edge, and vice versa, in order to fulfill the $r_H = (1 \cdots 2)$ condition. As a consequence, the model parameter μ_0, representing the intrinsic band mobility, is wrongly determined. Therefore, the knowledge of some parameter values from additional measurements (e.g., effective mass from free-carrier absorption, total carrier concentration from capacitance-voltage measurements) is helpful for increasing the confidence level of the fit parameters when evaluating the electron transport data. In order to adequately cope with this, we particularly take care that the obtained fit parameters yield total carrier concentrations that are consistent with measured approximate values from capacitance-voltage measurements, if available. For the calculation of n_{total} the assumed value for the characteristic energy of the exponential band tails E_0 of about 30 meV leads to reasonable results for all investigated AOS materials.

Another, more general, inherent issue of the model is the disregard of temperature-dependent scattering mechanisms, which leads to the assumption that the intrinsic band mobility μ_0, and accordingly the Hall-scattering factor, are temperature independent. Actually, this is only for highly degenerate oxide semiconductors a good assumption. But we note that, whereas an understanding of different scattering mechanisms in crystalline multication compounds like *c*-IGZO already exists [55,56], the contribution to the drift mobility in AOSs is more unclear due to the complexity of transport phenomena [57].

Further, the assumption that the fluctuating mobility edge E_m can be described by a Gaussian distribution could be insufficient. Particularly for multicomponent AOS materials with varying cation composition, it is possible that the potential fluctuations are not Gaussian normally distributed due to cation clustering. It is worthwhile to note, in AOSs a conventional mobility edge, as defined for covalent amorphous semiconductors, which clearly separates localized from extended states, does not exist. More specifically, the assumption that all conduction-band tail electrons are localized and therefore do not contribute to conductivity is not realistic for AOSs. In fact, the electrons in the exponential conduction-band tail states of AOSs are at most weakly localized [57,58]. Also, the assumed exponential distribution of localized tail states can be questioned at all. Actually, theoretical and experimental studies report fully occupied, Gaussian-shaped, localized deep-subgap states originating from undercoordinated atoms and exponential band tailing due to structural disorder in AOSs [33]. To solve these questions and to further improve the quantitative description of charge transport in AOS materials, a more reliable knowledge about the local microscopic and electronic structure and its influence on scattering mechanisms in AOSs, particularly for multianion compounds, is essential. Certainly, due to the complex nature of the investigated AOSs this remains challenging.

VI. CONCLUSION

The presented extended percolation-based random band-edge model is adequate for quantitative modeling of the experimentally determined temperature dependence of Hall mobility and carrier concentration of all investigated AOS materials, namely multication *a*-IGZO and *a*-ZTO, multianion *a*-ZnON and multinary Zn-Mg-ON. The necessary introduction of the Hall-scattering factor is proven to result in reasonable band-disorder parameters after several parameter correlations of the model are figured out. Moreover, the observed parameter trends in dependence on growth conditions can be interpreted in accordance with the current state of research. In particular, for *a*-ZTO we find a standard deviation of the mobility edge distribution ranging between 20 to 60 meV, which increases with increasing Sn content and decreases with increasing oxygen partial deposition pressure. For the single-cation compound *a*-ZnON the mobility edge is expectedly less spatially distributed with the standard deviation increasing from 23 to 36 meV with increasing deposition temperature. For the multinary compound Zn-Mg-ON we find that the addition of magnesium cations leads to an increase in standard deviation from 20 to 40 meV for the mobility edge distribution. In addition, for the latter two it turns out that localized tail states below the mobility edge are crucial factors for the charge-transport description and cannot be neglected, contrary to the findings for the multication compounds *a*-IGZO and *a*-ZTO, which is in agreement with the expectations and experimental findings, respectively. Thus, evaluating the temperature-dependent Hall-effect

thin-film data of AOSs within this model provides a valuable tool for elucidating the effect of anionic and cationic disorder on the electronic structure of the conduction-band minimum and as such contributes to a profound understanding of charge transport in AOSs, which in turn could aid enhancing device performance. Even more, it is possible to gain insights into the influence of process parameters if device processing is not yet successful and allows for tuning the desired properties once the relationship between process parameters and Hall-effect data is systematically analyzed.

ACKNOWLEDGMENTS

The authors acknowledge P. Schlupp for ZTO thin-film deposition and valuable discussions. This work is funded by Deutsche Forschungsgemeinschaft within the framework of the ANR-DFG project *Zinc Magnesium Oxynitrides (ZONE)* (GR 1011/36-1). A.W and O.H. further acknowledge the Leipzig School of Natural Sciences BuildMoNa and we acknowledge support from Leipzig University for Open Access Publishing.

[1] H. Hosono, Ionic amorphous oxide semiconductors: Material design, carrier transport, and device application, J. Non-Cryst. Solids **352**, 851 (2006).

[2] H. Q. Chiang, J. F. Wager, R. L. Hoffman, J. Jeong, and D. A. Keszler, High mobility transparent thin-film transistors with amorphous zinc tin oxide channel layer, Appl. Phys. Lett. **86**, 013503 (2005).

[3] Y. Ye, R. Lim, and J. M. White, High mobility amorphous zinc oxynitride semiconductor material for thin film transistors, J. Appl. Phys. **106**, 074512 (2009).

[4] P. Schlupp, F.-L. Schein, H. von Wenckstern, and M. Grundmann, All amorphous oxide bipolar heterojunction diodes from abundant metals, Adv. Electron. Mater. **1**, 1400023 (2015).

[5] P. Schlupp, H. von Wenckstern, and M. Grundmann, Schottky barrier diodes based on room temperature fabricated amorphous zinc tin oxide thin films, Phys. Status Solidi (a) **214**, 1700210 (2017).

[6] G. T. Dang, T. Kawaharamura, M. Furuta, and M. W. Allen, Zinc tin oxide metal semiconductor field effect transistors and their improvement under negative bias (illumination) temperature stress, Appl. Phys. Lett. **110**, 073502 (2017).

[7] S. Vogt, H. von Wenckstern, and M. Grundmann, MESFETs and inverters based on amorphous zinc-tin-oxide thin films prepared at room temperature, Appl. Phys. Lett. **113**, 133501 (2018).

[8] O. Lahr, Z. Zhang, F. Grotjahn, P. Schlupp, S. Vogt, H. von Wenckstern, A. Thiede, and M. Grundmann, Full-swing, high-gain inverters based on ZnSnO JFETs and MESFETs, IEEE Trans. Electron Devices **66**, 3376 (2019).

[9] P. Schlupp, S. Vogt, H. von Wenckstern, and M. Grundmann, Low voltage, high gain inverters based on amorphous zinc tin oxide on flexible substrates, APL Mater. **8**, 061112 (2020).

[10] O. Lahr, S. Vogt, H. von Wenckstern, and M. Grundmann, Low-voltage operation of ring oscillators based on room-temperature-deposited amorphous zinc-tin-oxide channel MESFETs, Adv. Electron. Mater. **5**, 1900548 (2019).

[11] A. Reinhardt, H. von Wenckstern, and M. Grundmann, Metal–semiconductor field-effect transistors based on the amorphous multi-anion compound ZnON, Adv. Electron. Mater. **6**, 1901066 (2020).

[12] A. Reinhardt, H. von Wenckstern, and M. Grundmann, All-amorphous junction field-effect transistors based on high-mobility zinc oxynitride, Adv. Electron. Mater. **7**, 2000883 (2021).

[13] S. Lee, K. Ghaffarzadeh, A. Nathan, J. Robertson, S. Jeon, C. Kim, I.-H. Song, and U.-I. Chung, Trap-limited and percolation conduction mechanisms in amorphous oxide semiconductor thin film transistors, Appl. Phys. Lett. **98**, 203508 (2011).

[14] W. C. Germs, W. H. Adriaans, A. K. Tripathi, W. S. C. Roelofs, B. Cobb, R. A. J. Janssen, G. H. Gelinck, and M. Kemerink, Charge transport in amorphous InGaZnO thin-film transistors, Phys. Rev. B **86**, 155319 (2012).

[15] C.-G. Lee, B. Cobb, and A. Dodabalapur, Band transport and mobility edge in amorphous solution-processed zinc tin oxide thin-film transistors, Appl. Phys. Lett. **97**, 203505 (2010).

[16] J.-T. Li, L.-C. Liu, J.-S. Chen, J.-S. Jeng, P.-Y. Liao, H.-C. Chiang, T.-C. Chang, M. I. Nugraha, and M. A. Loi, Localized tail state distribution and hopping transport in ultrathin zinc-tin-oxide thin film transistor, Appl. Phys. Lett. **110**, 023504 (2017).

[17] S. Lee, A. Nathan, Y. Ye, Y. Guo, and J. Robertson, Localized tail states and electron mobility in amorphous ZnON thin film transistors, Sci. Rep. **5**, 13467 (2015).

[18] S. Baranovski, ed., *Charge Transport in Disordered Solids with Applications in Electronics* (John Wiley & Sons Ltd., 2006).

[19] I. I. Fishchuk, A. Kadashchuk, A. Bhoolokam, A. de Jamblinne de Meux, G. Pourtois, M. M. Gavrilyuk, A. Köhler, H. Bässler, P. Heremans, and J. Genoe, Interplay between hopping and band transport in high-mobility disordered semiconductors at large carrier concentrations: The case of the amorphous oxide InGaZnO, Phys. Rev. B **93**, 195204 (2016).

[20] K. Nomura, H. Ohta, A. Takagi, T. Kamiya, M. Hirano, and H. Hosono, Room-temperature fabrication of transparent flexible thin-film transistors using amorphous oxide semiconductors, Nature **432**, 488 (2004).

[21] T. Kamiya, K. Nomura, and H. Hosono, Electronic structures above mobility edges in crystalline and amorphous In-Ga-Zn-O percolation conduction examined by analytical model, J. Disp. Technol. **5**, 462 (2009).

[22] A. Takagi, K. Nomura, H. Ohta, H. Yanagi, T. Kamiya, M. Hirano, and H. Hosono, Carrier transport and electronic structure in amorphous oxide semiconductor, a-$InGaZnO_4$, Thin Solid Films **486**, 38 (2005).

[23] T. Kamiya, K. Nomura, and H. Hosono, Origin of definite hall voltage and positive slope in mobility-donor density

relation in disordered oxide semiconductors, Appl. Phys. Lett. **96**, 122103 (2010).
[24] M. Kimura, T. Kamiya, T. Nakanishi, K. Nomura, and H. Hosono, Intrinsic carrier mobility in amorphous In-Ga-Zn-O thin-film transistors determined by combined field-effect technique, Appl. Phys. Lett. **96**, 262105 (2010).
[25] D. Adler, L. P. Flora, and S. D. Senturia, Electrical conductivity in disordered systems, Solid State Commun. **12**, 9 (1973).
[26] A. V. Nenashev, J. O. Oelerich, S. H. M. Greiner, A. V. Dvurechenskii, F. Gebhard, and S. D. Baranovskii, Percolation description of charge transport in amorphous oxide semiconductors, Phys. Rev. B **100**, 125202 (2019).
[27] S. D. Baranovskii, A. V. Nenashev, J. O. Oelerich, S. H. M. Greiner, A. V. Dvurechenskii, and F. Gebhard, Percolation description of charge transport in the random barrier model applied to amorphous oxide semiconductors, EPL (Europhysics Letters) **127**, 57004 (2019).
[28] B. I. Shklovskii and A. L. Efros, *Electronic Properties of Doped Semiconductors* (Springer Berlin Heidelberg, 1984).
[29] See Supplementary Material at http://link.aps.org/supplemental/10.1103/PhysRevApplied.17.024007 for a detailed theoretical description of the RBE model from Nenashev *et al.* [26] and the extended RBE model, for more information about the implementation of the optimization routine, an additional multisample fit of the *a*-IGZO Hall-effect data and a single sample fit of the *a*-IGZO conductivity data. Moreover, additional information about the influence of the temperature dependence of the Fermi level and the influence of the Hall-scattering factor are given.
[30] A. Y. Shik, Hall effect and electron mobility in inhomogeneous semiconductors, JETP Lett. **20**, 5 (1974).
[31] M. Grundmann, *The Physics of Semiconductors: An Introduction Including Nanophysics and Applications* (Springer International Publishing, 2021).
[32] D. K. Schroder, *Semiconductor Material and Device Characterization* (John Wiley & Sons, Inc., 2006).
[33] K. Ide, K. Nomura, H. Hosono, and T. Kamiya, Electronic defects in amorphous oxide semiconductors: A review, Phys. Status Solidi (a) **216**, 1800372 (2019).
[34] E. Lee, T. Kim, A. Benayad, H. Kim, S. Jeon, and G.-S. Park, Ar plasma treated ZnON transistor for future thin film electronics, Appl. Phys. Lett. **107**, 122105 (2015).
[35] J. Gwang Um, M. Mativenga, P. Migliorato, and J. Jang, Increase of interface and bulk density of states in amorphous-indium-gallium-zinc-oxide thin-film transistors with negative-bias-under-illumination-stress time, Appl. Phys. Lett. **101**, 113504 (2012).
[36] Y. Sonand and R. L. Peterson, The effects of localized tail states on charge transport mechanisms in amorphous zinc tin oxide schottky diodes, Semicond. Sci. Technol. **32**, 12LT02 (2017).
[37] A. Reinhardt, H. Frenzel, H. von Wenckstern, D. Spemann, and M. Grundmann, Electron transport mechanism in rf-sputtered amorphous zinc oxynitride thin films, Phys. Status Solidi (a) **213**, 1767 (2016).
[38] A. Welk, A. Reinhardt, O. Herrfurth, T. Schultz, H. von Wenckstern, N. Koch, and M. Grundmann, Tuning material properties of amorphous zinc oxynitride thin films by magnesium addition, APL Mater. **9**, 021120 (2021).
[39] S. Bitter, P. Schlupp, M. Bonholzer, H. von Wenckstern, and M. Grundmann, Influence of the cation ratio on optical and electrical properties of amorphous zinc-tin-oxide thin films grown by pulsed laser deposition, ACS Comb. Sci. **18**, 188 (2016).
[40] G. Hautier, A. Miglio, D. Waroquiers, G.-M. Rignanese, and X. Gonze, How does chemistry influence electron effective mass in oxides? A high-throughput computational analysis, Chem. Mater. **26**, 5447 (2014).
[41] Y. Sato, J. Kiyohara, A. Hasegawa, T. Hattori, M. Ishida, N. Hamada, N. Oka, and Y. Shigesato, Study on inverse spinel zinc stannate, Zn_2SnO_4, as transparent conductive films deposited by rf magnetron sputtering, Thin Solid Films **518**, 1304 (2009).
[42] J. Lee, D.-Y. Cho, J. Jung, U. K. Kim, S. H. Rha, C. S. Hwang, and J.-H. Choi, Theoretical and experimental studies on the electronic structure of crystalline and amorphous $ZnSnO_3$ thin films, Appl. Phys. Lett. **102**, 242111 (2013).
[43] S. C. Siah, S. W. Lee, Y. S. Lee, J. Heo, T. Shibata, C. U. Segre, R. G. Gordon, and T. Buonassisi, X-ray absorption spectroscopy elucidates the impact of structural disorder on electron mobility in amorphous zinc-tin-oxide thin films, Appl. Phys. Lett. **104**, 242113 (2014).
[44] W. Körner and C. Elsässer, Density-functional theory study of stability and subgap states of crystalline and amorphous Zn-Sn-O, Thin Solid Films **555**, 81 (2014).
[45] M. J. Wahila, Z. W. Lebens-Higgins, K. T. Butler, D. Fritsch, R. E. Treharne, R. G. Palgrave, J. C. Woicik, B. J. Morgan, A. Walsh, and L. F. J. Piper, Accelerated optimization of transparent, amorphous zinc-tin-oxide thin films for optoelectronic applications, APL Mater. **7**, 022509 (2019).
[46] J. Park, Y. S. Kim, K.-C. Ok, Y. C. Park, H. Y. Kim, J.-S. Park, and H.-S. Kim, A study on the electron transport properties of ZnON semiconductors with respect to the relative anion content, Sci. Rep. **6**, 24787 (2016).
[47] F. Xian, J. Ye, S. Gu, H. H. Tan, and C. Jagadish, Structural transition, subgap states, and carrier transport in anion-engineered zinc oxynitride nanocrystalline films, Appl. Phys. Lett. **109**, 023109 (2016).
[48] J. T. Jang, H. Kang, H. R. Yu, E. S. Kim, K. S. Son, S.-H. Cho, D. M. Kim, S.-J. Choi, and D. H. Kim, The influence of anion composition on subgap density of states and electrical characteristics in ZnON thin-film transistors, IEEE Electron Device Lett. **40**, 40 (2019).
[49] H.-S. Kim, S. H. Jeon, J. S. Park, T. S. Kim, K. S. Son, J.-B. Seon, S.-J. Seo, S.-J. Kim, E. Lee, J. G. Chung, H. Lee, S. Han, M. Ryu, S. Y. Lee, and K. Kim, Anion control as a strategy to achieve high-mobility and high-stability oxide thin-film transistors, Sci. Rep. **3**, 1459 (2013).
[50] C.-Y. Jeong, H.-J. Kim, D.-H. Kim, H.-S. Kim, T. S. Kim, J.-B. Seon, S. Lee, D. H. Kim, and H.-I. Kwon, Investigation of carrier transport mechanism in high mobility ZnON thin-film transistors, IEEE Electron Device Lett. **37**, 1570 (2016).
[51] H.-J. Jeong, H.-M. Lee, K.-C. Ok, J. Park, and J.-S. Park, Supreme performance of zinc oxynitride thin film transistors via systematic control of the photo-thermal activation process, J. Materi. Chem. C **6**, 5171 (2018).

[52] J. T. Jang, H.-D. Kim, D. M. Kim, S.-J. Choi, H.-S. Kim, and D. H. Kim, Effect of anion composition on the bias stress stability in Zn-O-N thin-film transistors, IEEE Electron Device Lett. **41**, 1376 (2020).

[53] J. Lu, S. Fujita, T. Kawaharamura, H. Nishinaka, Y. Kamada, and T. Ohshima, Carrier concentration induced band-gap shift in Al-doped $Zn_{1-x}Mg_xO$ thin films, Appl. Phys. Lett. **89**, 262107 (2006).

[54] C. Franz, M. Giar, M. Heinemann, M. Czerner, and C. Heiliger, Band structure and effective masses of $Zn_{1-x}Mg_xO$, MRS Proc. **1494**, 57 (2012).

[55] Y. Kang, Y. Cho, and S. Han, Cation disorder as the major electron scattering source in crystalline InGaZnO, Appl. Phys. Lett. **102**, 152104 (2013).

[56] Y. Jegal, A. H. Kulahlioglu, C.-K. Baek, and B. D. Kong, Disorder originated unusual mobility in crystalline $InGaZnO_4$, IEEE Electron Device Lett. **41**, 872 (2020).

[57] J. E. Medvedeva, D. B. Buchholz, and R. P. H. Chang, Recent advances in understanding the structure and properties of amorphous oxide semiconductors, Adv. Electron. Mater. **3**, 1700082 (2017).

[58] J. Robertson, Disorder and instability processes in amorphous conducting oxides, Phys. Status Solidi (b) **245**, 1026 (2008).